BRNO UNIVERSITY OF TECHNOLOGY
VYSOKÉ UČENÍ TECHNICKÉ V BRNĚ

FACULTY OF MECHANICAL ENGINEERING
FAKULTA STROJNÍHO INŽENÝRSTVÍ

INSTITUTE OF PHYSICAL ENGINEERING
ÚSTAV FYZIKÁLNÍHO INŽENÝRSTVÍ

EVALUATION OF DIFFERENT DIELECTRICS FOR MID-INFRARED WAVEGUIDES
VYHODNOCENÍ VLASTNOSTÍ DIELETRIK PRO VLNOVODY VE STŘEDNÍ INFRAČERVENÉ OBLASTI

BACHELOR'S THESIS
BAKALÁŘSKÁ PRÁCE

AUTHOR — Aleš Konečný
AUTOR PRÁCE

SUPERVISOR — Dr.techn. Ing. Hermann Detz
VEDOUCÍ PRÁCE

BRNO 2019

BRNO UNIVERSITY OF TECHNOLOGY
FACULTY OF MECHANICAL ENGINEERING

Bachelor's Thesis Assignment

Institut:	Institute of Physical Engineering
Student:	**Aleš Konečný**
Degree programm:	Applied Sciences in Engineering
Branch:	Physical Engineering and Nanotechnology
Supervisor:	**Dr.techn. Ing. Hermann Detz**
Academic year:	2018/19

As provided for by the Act No. 111/98 Coll. on higher education institutions and the BUT Study and Examination Regulations, the director of the Institute hereby assigns the following topic of Bachelor's Thesis:

Evaluation of Different Dielectrics For Mid-Infrared Waveguides

Brief description:

This work focuses on dielectric and plasmonic waveguides, which can be used as on-chip interconnects between laser and detector at mid-infrared wavelengths. Proof of principle demonstrations used stacks of Au and SiN to guide surface plasmon polariton modes. The goal of this thesis is to identify, fabricate and characterize dielectric materials, which provide low optical losses and which can be combined with established InP-based sensor chips.

Bachelor's Thesis goals:

Identification of several candidate dielectrics.
Fabrication of dielectric and metal/dielectric layer stacks.
Optical characterization of these materials.

Recommended bibliography:

MIZAIKOFF, B. Waveguide-enhanced mid-infrared chem/bio sensors. Chemical Society Reviews. 2013, 42(22)

SIEGER, M. a MIZAIKOFF, B. Toward On-Chip Mid-Infrared Sensors. Analytical Chemistry. 2016, 88(11), 5562-5573

SCHWARZ, B., REININGER, P., DETZ, H., ZEDERBAUER, T., ANDREWS, A., SCHRENK, W., STRASSER, G. Monolithically Integrated Mid-Infrared Quantum Cascade Laser and Detector. Sensors. 2013, 13(2), 2196-2205

Abstrakt

Využití plasmonovo polaritonových vlnovodů se ukázalo vhodné pro senzorové aplikace ve středně infračervené oblasti spektra. Vlnovod je v kontaktu s médiem v plynném či kapalném stavu, který obsahuje měřenou koncentraci hledané látky. Při šíření elektromagnetického vzruchum jsou na něj kladeny podmínky nízkých ztrát a dostatečné interakce s médiem. Tyto podmínky jsou splněny, je-li na kov nanesena tenká dielektrická vrstva. Tato práce je zaměřena na dielektrika na bázi křemíku. Součástí práce byla výroba vícevrstevnatých vlnovodů technikou plazmaticky vylepšené chemické depozice, magnetronového naprašování a metodou fotolitografie. Nanášení vrstev probíhalo na obvykle užívané Si substráty. Hodnocení dielektrických vrstev a výrobních metod probíhá na základě elipsometrických měření indexu lomu a absorbce v infračervené oblasti spektra.

Abstract

The utilization of plasmon polariton waveguides for mid-infrared light has proven its suitability for sensor applications. The waveguide can be surrounded by a gaseous or liquid phase medium, which contains an analyte substance of which the concentration can be measured. The electromagnetic field propagates along the waveguide, which has to satisfy low losses and sufficient interaction conditions. These are fulfilled using a thin dielectric layer applied on a metal surface. This thesis is focused on Si-based dielectrics. Within this work, multilayer waveguides were fabricated by high vacuum magnetron sputtering, plasma-enhanced vapor deposition and photolithography. The deposition was carried out on commonly used Si substrates and is ready to be transfered to InP-based chips. Evaluation of dielectric layers and fabrication methods are based on ellipsometric measurements of refractive index and extinction coefficient in the infrared spectrum.

Klíčová slova

středně infračervená, vlnovod, dielektrika, naprašování, pecvd

Keywords

mid infrared, waveguide, dielectrics, sputtering, pecvd

KONEČNÝ, A. *Evaluation of Different Dielectrics for Mid-Infrared Waveguides.* Brno: Vysoké učení technické v Brně, Fakulta strojního inženýrství, 2019. 32 s. Supervisor Dr.techn. Ing. Hermann Detz.

I declare that I have elaborated my bachelor's thesis on the theme "'Evaluation of different dielectrics for Mid-Infrared waveguides"' independently, under the supervision of bachelor's thesis supervisor and with the use of technical literature and other sources of information which are all quoted in the thesis and detailed in the list of literature at the end of the thesis.

Aleš Konečný

I am very grateful to my supervisor Dipl-Ing. Dr.techn. Hermann Detz, for his time, effort, kindness, help and all valuable advices he has given to me. My thanks belong to Ing. Martin Hrtoň for helping me with Lumerical simulations, RNDr. Alois Nebojsa for his advices about ellipsometric data processing and Mgr. Marek Eliáš, PhD. for technical support during depositions. I would also like to acknowledge, that this work was carried out with the support of CEITEC Nano Research Infrastructure (ID LM2015041, MEYS CR, 2016–2019), CEITEC Brno University of Technology.

Aleš Konečný

Contents

Introduction

Mid-Infrared spectroscopy covers the spectral range from approximately 2.5 to 20 μm [1]. It provides discriminatory information due to the excitation of vibrational and rotational transitions, that are characteristic of numerous molecules. Individual molecules can be fingerprinted through the unique pattern of absorption lines, hence mid-infrared spectroscopy is successfully used for sensor application [2]. There are many design possibilities for such a spectrometer. Of particular interest are those, that are capable of working in hard-to-reach areas, where access to electricity and laboratory equipment cannot be relied upon. These usually consist of laser, detector and waveguide placed in between, serving as a light conductor and region of interaction with examined environment [1]. Recent progress in a field of lasers [3] and trends in overall device miniaturization [4] escalate demands for waveguide functionality.

This work targets appropriate materials for a waveguide application, which is the main criterion for its assessment. The thesis is divided into three chapters. Whereas first describes sensor principles and requirements for waveguide materials, second covers their fabrication and characterization methods. The last one is focused on waveguide optimization, where can be found most of the results.

The main goal is to consider different dielectric materials for mid-infrared waveguides, compare available fabrication methods and assess optical properties of deposited layers. Of particular interest are silicon-based dielectrics, commonly used in electronics. Utilized materials are further evaluated in respect to the sensor application and combination with established InP-based sensor chips.

1. MIR-Waveguides

Under the term waveguide, one usually imagines a conduit guiding light with minimal losses over long distances. These waveguides are widely used in a form of optical fibres serving as a information transmitter. Not denying benefits of fibre optics, the thesis is focused on schemes, that take advantage of interaction with sample located in the vicinity of the waveguide itself. These work as an active transducer, rather than just a light conduit, perfectly suited for a sensor application.

1.1 Wave-guiding concepts

This work focuses on planar waveguides benefiting from simple on-chip implementation. Two different concepts will be presented. The evanescent field absorption and SPP (surface plasmon polariton) waveguide. They will be explained and compared in respect to the guiding efficiency and interaction with surroundings.

1.1.1 Evanescent field absorption waveguide

This concept works on the well known principle of TIR (total internal reflection). Light propagates through medium of higher refractive index than that of the surrounding material. If the incident angle φ meets the condition defined in Equation 1.1, total reflection occurs allowing a transfer of minimum losses.

$$\varphi \geq arcsin\left(\frac{n_2}{n_1}\right) \tag{1.1}$$

n_2 describes core whereas n_1 refractive index of adjacent medium. Electromagnetic field propagating inside the adjacent medium calls evanescent field. Its origin comes from the transmitted part of the wave and has in case of TIR exponentially decaying behaviour at increasing distance from material interface [2]. These are illustrated in Figure 1.1. For evanescent field penetration depth applies approximation formula:

$$d_p = \frac{\lambda}{2\pi\sqrt{{n_2}^2 sin^2\varphi - {n_1}^2}} \tag{1.2}$$

where λ corresponds to the wavelength of the light.

The evanescent field is attenuated if analyte molecules are found directly on the surface or within d_p, consequently weakening a signal in the waveguide. The absorption is measured by detector. The evanescent field absorption can be described via pseudo Beer–Lambert relationship,

$$A = (\epsilon c l)r = log\frac{I_0}{I} \tag{1.3}$$

where I_0 describes the initial intensity, I measured intensity, ϵ is the molar absorptivity, l interaction distance, r the fraction of the energy outside the waveguide and c the concentration of the absorbing substance [2].

The signal-to-noise ratio is improved by lowering the waveguide thickness. Total reflection occurs more frequently increasing the evanescent field intensity, which leads to the enhanced sensitivity [2]. However, the core thickness should not be lower than about a half of the light wavelength in the material, corresponding to the last eigenmode in vertical direction is, since the absence of eigenmodes inevitably leads to the massive damping rise.

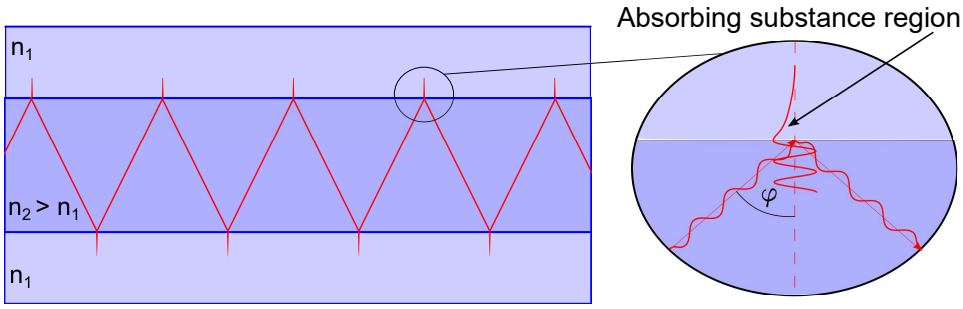

Figure 1.1: Schematic of a planar waveguide. Propagation demonstrated via TIR. Inset shows penetration outside the layer in the form of evanescent wave.

Further signal-to-noise improvements happen if the measured substance is applied to the vicinity of the waveguide, locally increasing its concentration. Nevertheless, planar evanescent field absorption waveguides are only suitable for investigated substances in liquid form, as the detection of gaseous molecules suffers from insufficient absorption, due to the short d_p distances [1].

1.1.2 SPP waveguide

The SPP waveguides on the other hand utilizes completely different principle. Electromagnetic wave propagating along the waveguide interacts with surface plasmons of metallic layer. A dielectric layer, directly deposited onto the metal, confines the interaction with evanescent decay over the distance from the interface [5]. An electromagnetic quasi-particle of coupled surface plasmon-photon transverse wave field on the interface between dielectric and metal calls polariton [6], hence the name, surface plasmon polariton waveguide.

The propagation distance, typically reaching units to tens of millimeters. It is increased by lateral confinement of a dielectric, creating the strip structure, while metal remains planar. These results were illustrated by Schwarz group for 0 to 500 nm thick and 20 to 200 μm wide SiN stripe on the top of the 400 nm thick Au layer [4].

The analyzed compound absorbs electromagnetic wave attenuating signal on the detector. Investigated concentration of absorbing substance, which allows to calculate the absorption, is calculated in the similar way to the previous case. It is worth mentioning, that most part of SPP waveguide mode is located outside, providing high interaction. Unlike planar evanescent field waveguides, SPPs work for liquid substances with low concentration of absorbent and may be used for gaseous molecules too.

In conclusion SPP waveguides sacrifice the guiding efficiency to the enhanced interaction with the sample. Since the concentration of analyzed substance in the waveguide

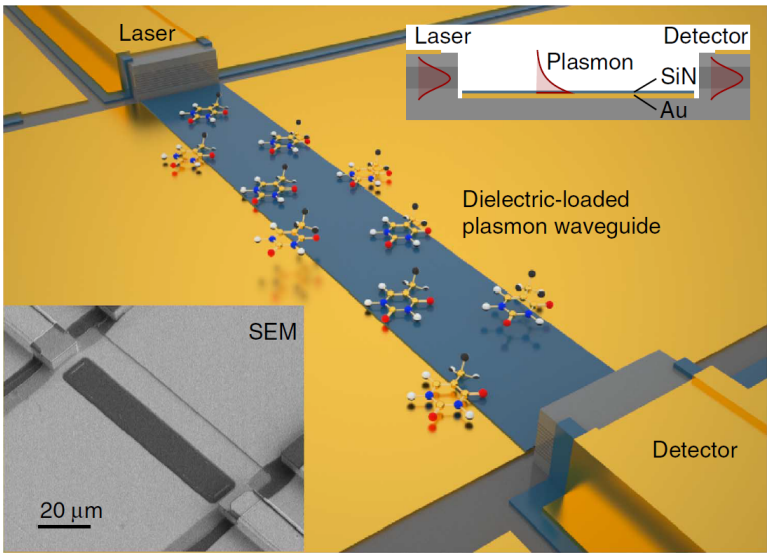

Figure 1.2: Monolithic mid-infrared on-chip sensor. The SPP waveguide is placed between laser and detector. The upper inset shows the cross section. The figure has been taken from [4].

vicinity commonly reaches low values and chip is usually smaller than units of centimeters, SPP is preferred technique over the evanescent field.
As a result, this thesis will strictly deal with the SPP waveguides in following pages.

1.2 Relevant materials

The SPP waveguide efficiency strongly depends on material choice. Most important features are optical properties of investigated substances, as they directly describe the optical behaviour in a volume and on a surface. Significant role plays dielectric function. Assuming a nonmagnetic isotropic medium, the electromagnetic equation is:

$$\mu_0 \frac{\partial^2 D}{\partial t^2} = \nabla^2 E \tag{1.4}$$

where μ_0 describes permeability in vacuum, D electric inductivity and E electric field. The solution is expected in a form of $E \propto exp(-i\omega t)exp(i\mathbf{Kr})$ and $D = \epsilon(\omega,\mathbf{K})E$. Substitution into the electromagnetic equation forms dispersion relation for electromagnetic waves:

$$\epsilon(\omega,\mathbf{K})\epsilon_0\mu_0\omega^2 = K^2 \tag{1.5}$$

where $\mathbf{K}$ is a vector of wavenumber and K its size, ω describes the angular frequency, $\mathbf{r}$ position, t time and $\epsilon(\omega,\mathbf{K})$ dielectric function. The equation could be modified into the optical formula [6]:

$$\epsilon(\omega) = N^2(\omega) = n^2 - k^2 + 2ink \tag{1.6}$$

Whereas $\epsilon(\omega)$ is generally complex value, refractive index n and extinction coefficient k are real. For $n > k$ the real part of $\epsilon(\omega)$ is positive, which means the electromagnetic wave propagates through the material with periodical amplitude, while for $k > n$, negative $\epsilon(\omega)$ results exponential damping [6]. The first case is common for dielectric

materials while the second for conductors, typically metals [5]. In the following lines, properties of materials for SPP waveguide application will be evaluated. The optical values strongly depend on used wavelength determined by the relationship:

$$\lambda \propto \frac{1}{K} \propto \frac{1}{\omega} \tag{1.7}$$

where λ resp. K represent wavelength resp. wavenumber in vacuum, while ω symbolize angular frequency independent on used medium. From this point λ only describes wavelength in vacuum ranging from 2.5 to 20 μm. This thesis is mostly concerned with values around 6.5 μm, where most of the MIR lasers & detectors work, due to their availability [4].

Substrate

In regards to the waveguides, substrate selection does not affect optical properties of whole waveguide much, since MIR penetration drops exponentially with increasing metallic layer thickness. Nevertheless, measurement of dielectric optical properties strongly depends on substrate choice, as dielectric layer is deposited directly onto the substrate. Considering price and simple fitting, silicon (100) from Siegert Wafer was selected. It is about 280 μm thick, p-doped with boron and single-side polished.

Metallic layer

The main criterion for metal is low absorption. Electromagnetic waves do not penetrate deep into the material, as $k > n$ results wave damping. Hence, the observation of surface properties like electric conductivity is critically important. Since SPPs vanish in the limit of a perfect electrical conductor [5], metals with lower conductivity are preferred. Aluminum is ideal candidate in terms of availability in research and industry, the propagation length is reduced due to the high conductivity and thin oxide layer is created under the atmospheric pressure, on the other hand, unlike gold, Al does not contaminate cells for following dielectric layer deposition. Thanks to the advantages described above, all waveguides made for the bachelor project utilizes Al as metallic layer.

Dielectric layer

Dielectric layer properties are more difficult to evaluate than metallic ones as the electromagnetic wave directly propagates through the dielectric medium. A higher refractive index n leads to reduced interaction with absorbent owing to more effective damping outside the waveguide. However, higher n increases the energy confinement in a perpendicular direction to the surface leading to the enhanced propagation length. As it turns out in upcoming pages, energy confinement can also be achieved by higher thickness. Yet, thicker dielectric films are undesirable due to the higher wave damping, hence materials with high refractive index n are preferred. On the other hand, the extinction coefficient k is much easier to evaluate. It should be simply as low as possible to reduce damping to the minimum. SiO_2 and Si_3N_4 are commonly used materials in industry and research. Utilizing SiO_2 as a waveguide has been demonstrated up to 5.18 μm [7] while Si_3N_4 has been investigated up to 8 μm [8].

These materials could be transparent for even longer wavelengths as will be discussed in following pages, First, it is important to qualitatively estimate deviation in the observed region. The deviation grows rapidly toward high wavelengths, due to the spectral radiance of a black body source [9]. The radiance on wavelength dependency is described via Planc's law,

$$B_\lambda(\lambda,T) = \frac{2hc^2}{\lambda^5}\frac{1}{e^{\frac{hc}{\lambda k_B T}} - 1} \tag{1.8}$$

where $B_\lambda(\lambda,T)$ refers to the amount of emitted energy for different wavelengths λ and source temperatures T. Mid-infrared sources often work for temperatures approaching 1000 K [10], hence relative radiance was calculated in the investigated wavelength range for 1000 K. This dependency is shown in Figure 1.3.

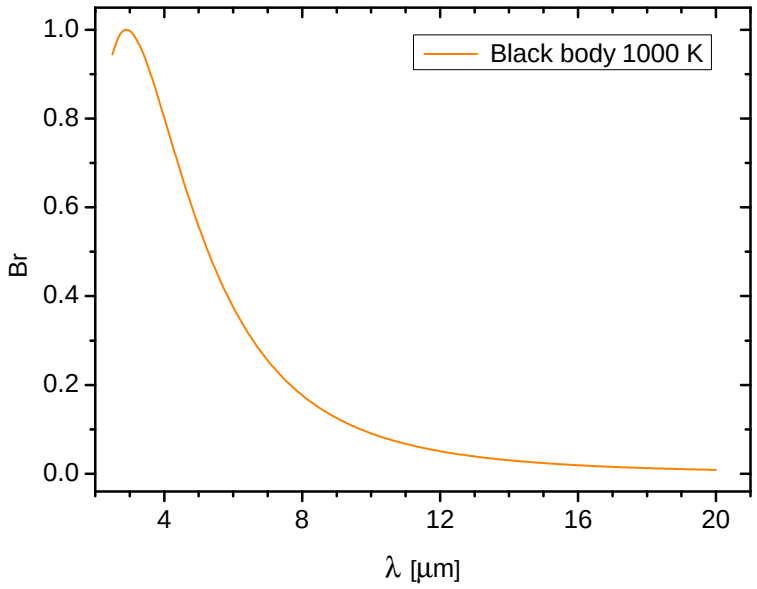

Figure 1.3: Black body source for 1000 K. The curve refers to the relative amount of energy B_r emitted at different radiation wavelengths λ.

The maximum occurs around 3 μm. For this value, the best signal-to-noise ratio is achieved. On the other hand, the lowest relative values can be found at highest wavelengths, referring to 20 μm. This means, that longer wavelengths are more affected than shorter ones. Still, regardless of the high deviation effect, region for high wavelengths is not studied anyway, since extinction coefficient reaches high values resulting material opacity as we see in Figure 1.4 and 1.5. Samples produced at TU Wien at 300 °C using PECVD (plasma-enhanced chemical vapor deposition) technique are compared to the Kischkat's database [11].

The wavelength has been plotted using non-lineral scale on horizontal axis to achieve constant horizontal distance between each point, since the ellipsometers used for this work measure at wavenumbers instead of wavelengths.

Measured values of SiO_2 correspond to the database. The material is transparent up to 6 μm. n and k amplitude does not reach its expected values, which could be resulted from high porosity. Yet, peaks occur at right wavelengths.

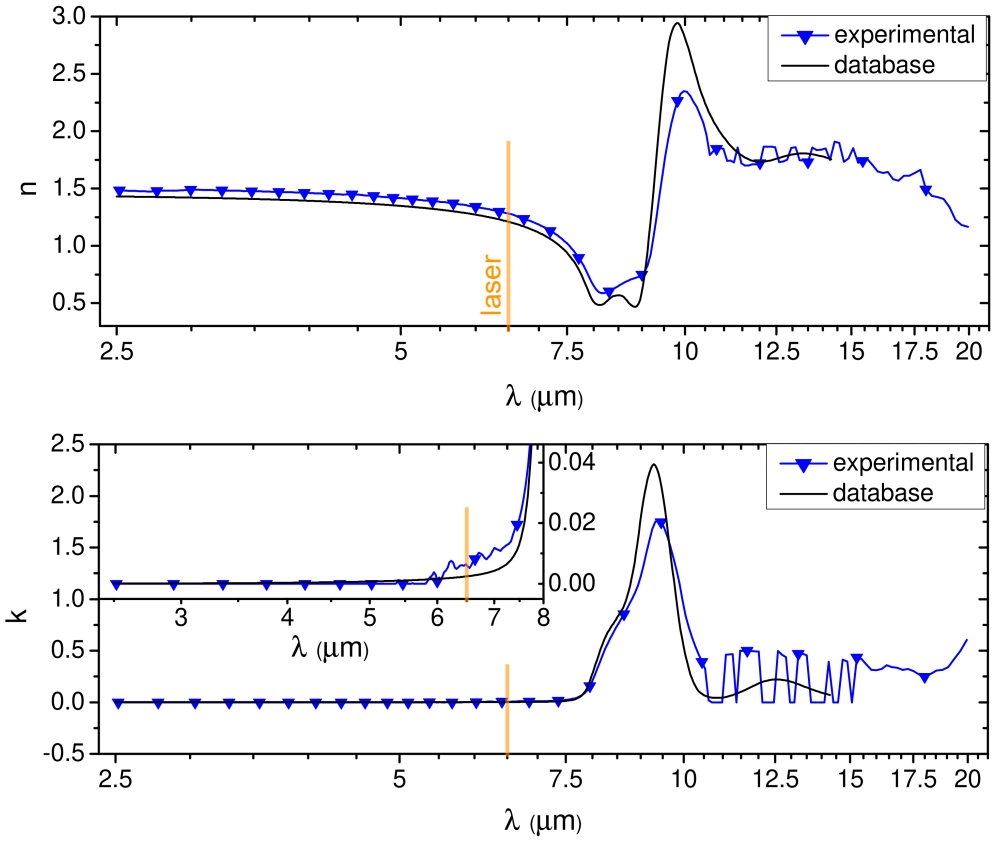

Figure 1.4: Thin layer measurement of SiO_2, deposited by PECVD technique at 300 °C in laboratories of TU Wien. The figure shows refractive index n and extinction coefficient k dependence on wavelength λ.

Si_3N_4 hardly meets expected values in regards to n. This deviation may be resulting from higher nitrogen concentration or occurrence of other contaminants in PECVD machine. Measured k roughly matches Kischkat's database. Nevertheless, in spite of anticipated values, transparency is achieved up to 7.3 μm.

1.3 Application in Sensors

In the previous sections the waveguide properties were discussed regardless of a laser and detector. This simplification is only justified for large dimensions or cases of separate construction. Recent miniaturization concepts or even single on-chip implementation often deal with shared substrate. Lasers and detectors are made of multilayer structure. To achieve discrete light source, required band gap has to be created, hence, individual layers are usually deposited by MBE (molecular beam epitaxy) technology. In these cases InP is commonly used laser substrate [4]. Since substrate for waveguides does not have to meet these strict requirements, InP could be simply shared for laser, detector and waveguide all at once.

Following paragraph is concerned with application of analyzed substances for MIR sensors. As discussed above, the excitation of vibrational and rotational transitions occurs in MIR. In ideal cases device is exposed to two substances with low and high absorption coefficient. Their quantity ratio is determined by absorbance via Pseudo Beer–Lambert relationship in Equation 1.3. In regards to the liquid substances, water

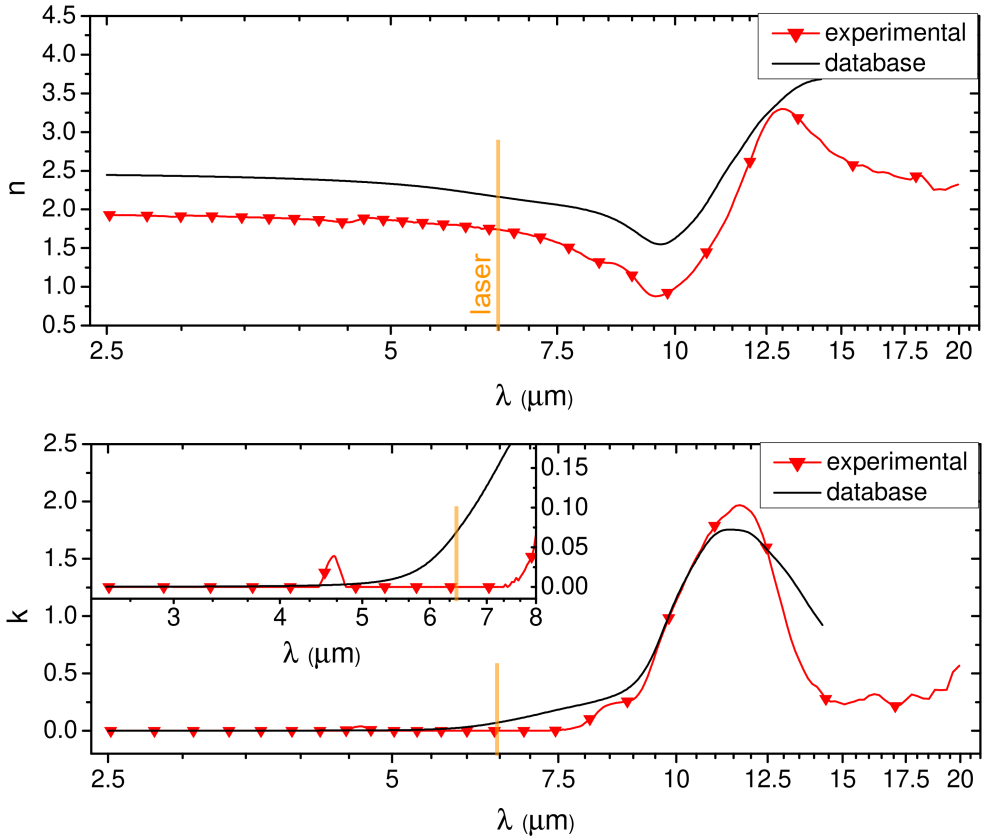

Figure 1.5: Thin layer measurement of Si_3N_4, deposited by PECVD technique at 300 °C in laboratories of TU Wien. The figure shows refractive index n and extinction coefficient k dependence on wavelength λ.

is usually observed as dominant absorbing substance, which shows to be the major limitation of MIR spectroscopy, since water-based solutions are the most common ones [1]. The sensor potential of on-chip implementation has been investigated for SPP waveguide and Quantum cascade laser detector [4], consisting of Quantum cascade laser and Quantum cascade detector in the same active region [3]. For the experiment, ethanol with low absorption and water with high absorption were used. The measurement at $\lambda = 6.5\,\mu$m showed great results down to the 17% water in ethanol solution [4]. In conclusion, water in ethanol detection is feasible option, however, the MIR sensor application does not only stand upon water-based solutions. Hollow waveguides are currently able to detect gaseous molecules for smoke detectors application or exhaled breath analysis. In addition biosensors for biomolecules detection such as proteins or DNA are expected in near future [1].

2. Nanofabrication and Characterization

2.1 Thin layer deposition

Thin layers refer to planar structures of thickness from tens of nanometers to several micrometers [12]. Deposition takes place under reduced-pressure environment to decrease layer contamination. Deposition of silicon-based thin films is one of the most developed in field. Since growing rate and simple usability is preferred over regular atomic structure, epitaxial growth techniques like MBE (molecular beam epitaxy) are not used. In addition, chosen technology should handle both metallic and dielectric layer deposition to prevent exposure to atmospheric pressure, as most metals oxidize outside a vacuum chamber.

This work focuses on two methods. Magnetron sputtering for Al and SiO_2 deposition, which benefits from high chemical purity and ability to sputter both metallic and dielectric layer inside the chamber, but suffers from low deposition rate and the commonly used PECVD (Plasma enhanced chemical vapor deposition) for SiO_2 and Si_3N_4. Its advantage is exact 1:2 silicon to oxygen ratio and high growing rate [13][14]. On the other hand PECVD is not suitable for metal deposition and suffers from contamination.

2.1.1 Magnetron sputtering

Magnetron sputtering is a physical vapor deposition method (PVD). The operation principle of this technique is to controllably transfer atoms from source to a substrate where film formation and growth proceed atomistically. In magnetron sputtering working gas is ionized by applied bias. Ferromagnets located under the target form a magnetic field in its surroundings, which forces electrons to move along helix trajectory with higher collision probability resulting amplified glow discharge density [15]. Impact of working gas ions enables atoms to dislodge from solid target surface, fly through plasma and settle on the substrate surface. The most common working gas source is argon. It does not chemically interact with target molecules since argon belongs to the inert gas family, furthermore it is relatively cheap.

Figure 2.1 represents basic principle of magnetron sputtering. Target is usually located at the bottom of the chamber whereas substrate is situated at the top. Dense plasma is found near above target, because of the limited magnetic field range. The biggest force upon electrons traveling directly to the target surface occurs on axis

in the middle between north and south magnetic pole, where electron velocity and magnetic field are perpendicular to each other. Since both ferromagnets and targets are rotationally symmetrical, atoms dislodge mainly from concentric circle of radius twice smaller than radius of target, forming distinctive wear annulus. Sputtered atoms form similar trace to the normal distribution. To achieve even distribution on substrate, target is tilted to aim to the 1/4 of the substrate diameter, while substrate steadily rotates along its axis.

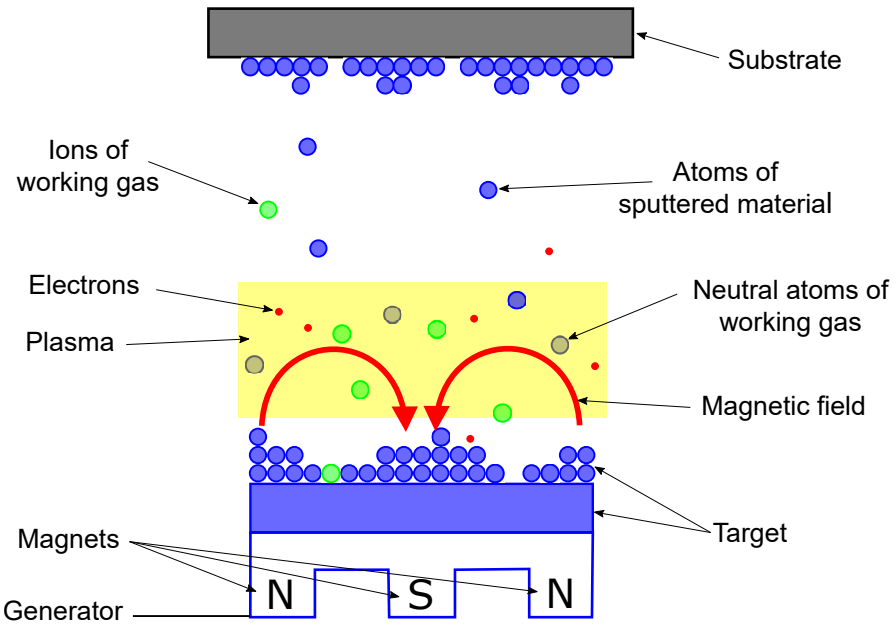

Figure 2.1: Schematic representation of magnetron sputtering principle

Applied bias is achieved by DC (direct current) or RF (radio frequency) generator.

DC generator

DC source is the most commonly used plasma generator for magnetron sputtering. At low voltage negligibly small current flows due to the small amount of initial charge carriers. As the voltage increases, more carriers are created because of ion collisions with cathode releasing secondary electrons and ionization of neutral atoms, both leading to the increased current. If the initial electrons consequently produce the same number of generated electrons, the discharge becomes self-sustaining and gas begins to glow. Further voltage increase leads to the "abnormal discharge" regime with nearly uniform current density over the target surface. [15]

Gas ionization may be enhanced by higher pressure too, as mean free path decreases and collision probability increases. However, sputtered atoms are scattered by collisions and deposition becomes insufficient [15], therefore higher pressure is only used for plasma ignition.

RF generator

DC sputtering can not be used for sputtering from insulating targets. Due to the high electrical resistivity, it fails to draw adequate current density. Instead of applying enormous voltage, alternative current at radio frequency is utilized. Frequency ranging

from 5 to 30 MHz meets the condition of ion immobilization and enables electrons to acquire enough energy to ionize neutral atoms. Since electrons are considerably more mobile than ions and easily follow periodic changes in electric field, positively charged electrode draw much more electron current than positive current by negatively charged electrode. As the AC (alternating current) generator is applied to the target, negatively charged initial current is drawn during first half of the cycle, unlike positively charged initial current during second half, which is considered to be insignificant. However, averaged value of the net current must not be different from zero owing to the system insulation. For this reason target has to be self-biased to a negative potential hence behaving like the cathode. [15]

2.1.2 PECVD

PECVD belongs to the chemical vapor deposition group (CVD). Volatile compounds chemically react with other gases to a nonvolatile solid that is automatically deposited on a suitably placed substrate [15], while gaseous products are pumped outside the chamber. Unlike standard CVD technique, PECVD utilizes ICP (inductively coupled plasma) to help to crack constituents of original gaseous molecule activating the chemical reaction, thus PECVD is able to operate at lower temperature.

Figure 2.2 shows simplified principle of PECVD technique. Substrate is usually located at the bottom of the chamber. Gas flows from the inlet at the top through the mesh securing uniform flux.

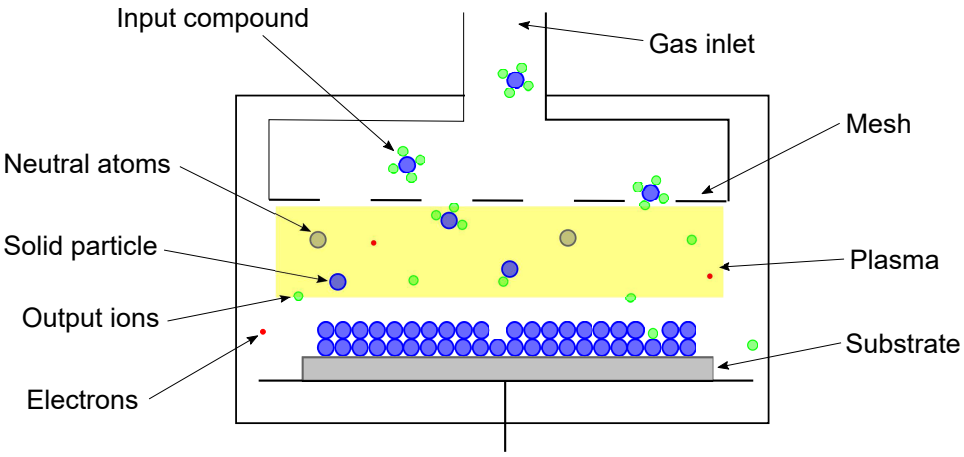

Figure 2.2: Schematic representation of PECVD principle

2.2 Lithography

The idea of this section is to demonstrate a simple way to create stripe structure waveguides. For this purpose, the microfabrication technique photolithography was chosen. This powerful tool utilizes optical masks with corresponding patterns, covering the certain area of top layer during an UV light exposition. First, a thin photosensitive layer called resist is uniformly applied on the sample by spincoating technique, heating then solidifies the semi-liquid resist. The sample is further exposed to the UV light. Mask from a non-translucent material prevents exposition to the resist area intended to remain or to be removed during consequent development, depending on the positive

or negative photolithography technique [16]. This demonstration has been carried out by positive photolithography, hence resist was removed from exposed area. In these places upper dielectric layer was etched using RIE (reactive ion etching). In the end resist was washed away by acetone. The whole process is illustrated in Figure 2.3.

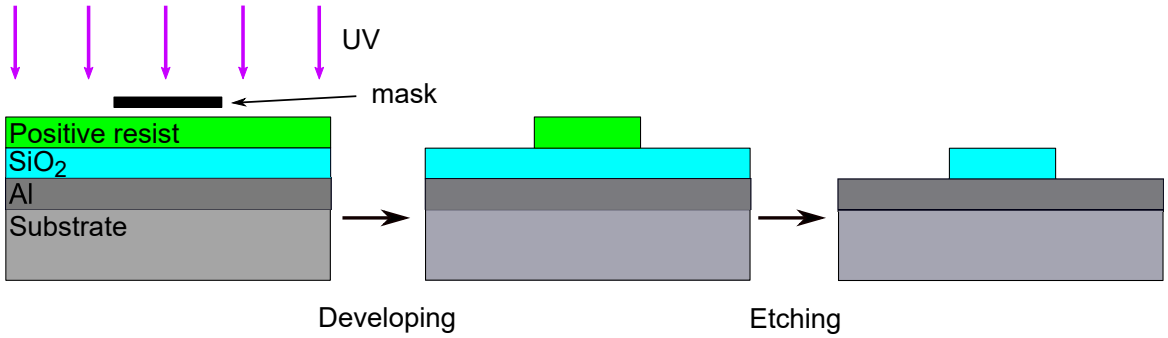

Figure 2.3: Strip structure fabrication by positive photolithography.

This work does not directly focus on waveguide fabrication, therefore, this process was not further optimized. In next step lithography imaging was executed. The utilized mask included several stripe structures of different width. For reasons discussed in upcoming chapter, stripe can be about 15 μm wide. The waveguide consists of Si wafer, Al metallic layer made by magnetron sputtering method and SiO_2 as a dielectric layer, made by PECVD at 100 °C. The material and choice of deposition technique had been also based on results discussed in following pages.

Images from electron microscope in Figure 2.4 show the Sinol structure. As metals discharge more observed secondary electrons than dielectric materials [17], dark stripes refer to aluminum covered with non-conductive dielectric layer, in this case SiO_2. Bright stripes on the other hand refer to a conductive Al layer surface. Image of a lithography confirms suitability of used technique, since sufficient quality was achieved. Cross section provides important information about thicknesses and layer quality. It shows four areas with three clear interfaces (right to left): Si wafer, Al layer, SiO_2 layer, Cu tape used to increase sample conductivity. Both deposited films approximately reach desired thickness of 100 nm, confirming correct deposition rates.

2.3 Ellipsometry

Spectroscopic ellipsometry is a powerful tool to characterize optical properties of different materials. At each wavelength, elliptically polarized light changes its polarization, as light is reflected from the sample surface. These are represented by Ψ and Δ [18], where:

$$tan\Psi \cdot e^{i\Delta} = \frac{R_p}{R_s} \tag{2.1}$$

R is the reflectance, which is calculated on material interface via Fresnel equations. Indexes s and p represent light polarization, where i and t report incident and transmission angle.

$$R_s = \left| \frac{n_1 \cdot cos\theta_i - n_2 \cdot cos\theta_t}{n_1 \cdot cos\theta_i + n_2 \cdot cos\theta_t} \right|^2 \qquad R_p = \left| \frac{n_2 \cdot cos\theta_i - n_1 \cdot cos\theta_t}{n_2 \cdot cos\theta_i + n_1 \cdot cos\theta_t} \right|^2 \tag{2.2}$$

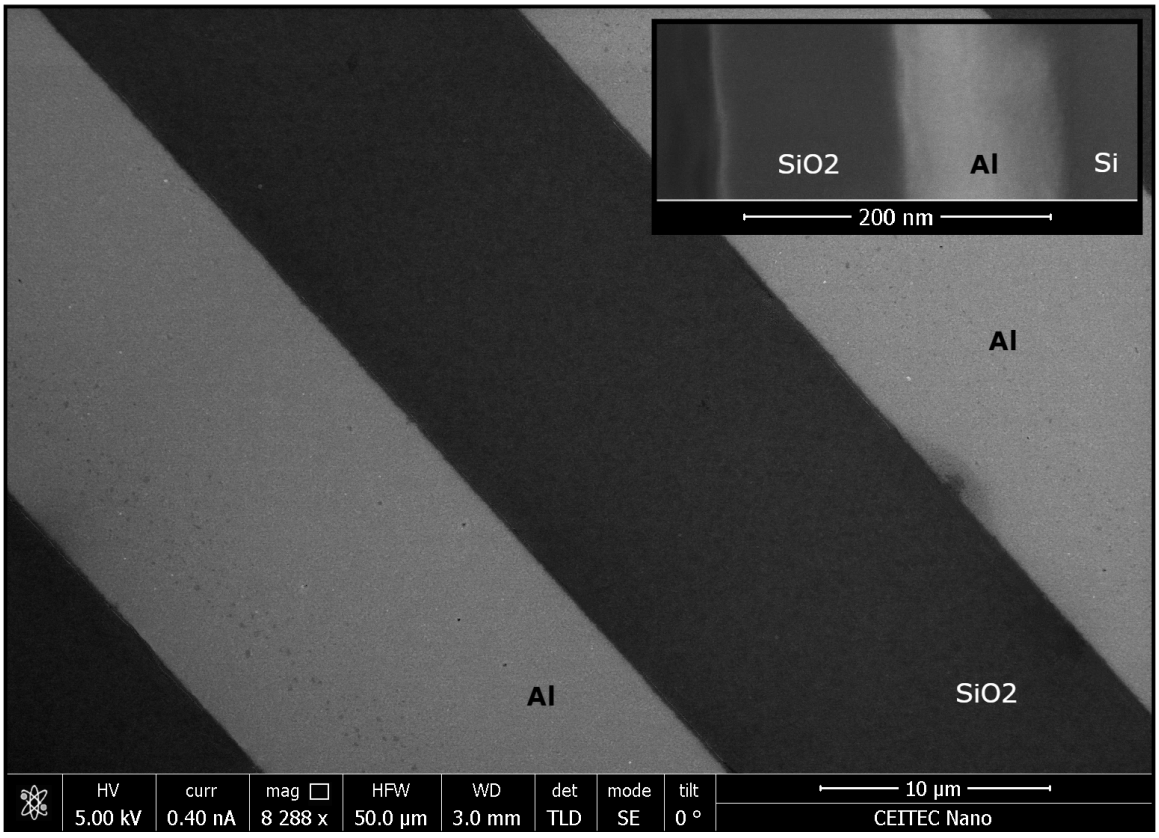

Figure 2.4: Electron microscope imaging of lithography strip structure. The inset in the upper right corner shows strip cross section.

Thus refractive index n and extinction coefficient k, as a product of wave damping, can be measured as a wavelength variable. The real power of ellipsometric measurement is demonstrated on thin layer sample showed in Figure 2.5.

If the layers are mostly transparent, the reflection occurs on each material interface, creating unique spectroscopic pattern, enabling to measure optical characteristics and thicknesses of any layer [19]. However, bear in mind, the more degrees of freedom system has, the more difficult the fitting gets and therefore it is important to find out as many pieces of information as possible.

2.3.1 VIS ellipsometry

The most measurements were made on thin dielectric layer samples directly deposited on the silicon substrate. First of all, visible spectroscopic scan was executed in order to determine the thin layer thickness. Infrared could be used as well, but the result would be affected by excitations [2] leading to inaccurate thickness estimation. Optical constants of the Si substrate were taken from laboratory database and remained fixed for following fitting. Substrate thickness was set to 0.28 mm, since thick layers absorb transmitted waves completely and therefore further increase would not affected the fit. Normal fit was executed with variable dielectric layer thickness and parameters A, B and C of the Cauchy relationship:

$$n(\lambda) = A + \frac{B}{\lambda^2} + \frac{C}{\lambda^4} \tag{2.3}$$

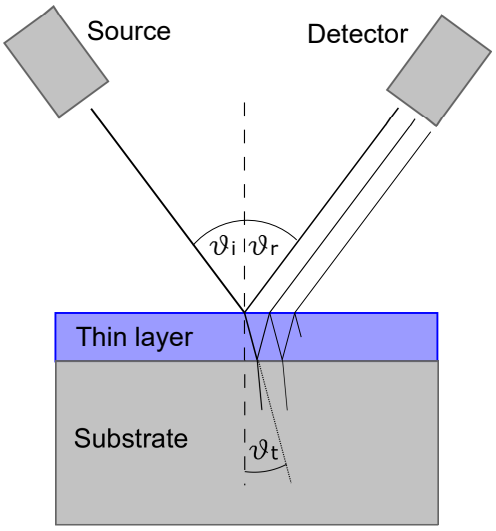

Figure 2.5: Reflection and transmission on thin film

MSE (mean square error) combined with slight changes in layer thickness when fitting at different wavelength ranges have been used to estimate thickness deviation. The results are showed in Table 2.1.

Table 2.1: Thickness estimation using VIS-Ellipsometry.

material	method	lab	T [°C]	t [nm]	Δt [nm]
SiO_2	pecvd	TU Wien	300	308	± 3.0
Si_3N_4	pecvd	TU Wien	300	314	± 2.0
Si_3N_4	pecvd NH3 free	TU Wien	300	318	± 3.0
SiO_2	magnetron	CEITEC	20	89.1	± 0.5
SiO_2	magnetron	CEITEC	100	81.5	± 0.5
SiO_2	pecvd	CEITEC	100	171	± 1.0
SiO_2	pecvd	CEITEC	200	140	± 1.0
Si_3N_4	pecvd	CEITEC	100	86	± 1.0
SiO_2	ald	CEITEC	200	44	± 1.0

In case of thicknesses greater than 100 nm damping is not negligible. Therefore, extinction component have been added to meet following equation [20]:

$$k(\lambda) = \alpha e^{1{,}24\beta(\frac{1}{\lambda}-\frac{1}{\gamma})} \tag{2.4}$$

whereas α and β were fit parameters and γ was set to constant value of 400 μm.

2.3.2 MIR ellipsometry

While VIS ellipsometry provides accurate thin layer thickness measurement, it does not say anything about optical properties in the area of interest. The "fingerprint" region, where most molecules have their vibrational and rotational excitation states, covers the range from 3 to 20 μm [3], therefore, MIR spectroscopic scan was performed.

The measurement was carried out for 3 incident angles, 70 °, 75 ° and 80 °. The refractive index n and extinction coefficient k correspondence between all angles confirms

sample position alignment, that is usually done in the beginning with laser. Experimental data are similar to the substrate optical values due to the small dielectric layer thickness. Subsequent fitting utilizes material database as the fixed or starting parameters. Si substrate optical values were chosen from Palik infrared database, created from generic oscillator and thickness was set to 0.28 mm. Dielectric optical values were also chosen from Palik infrared database, while thickness was set to the value measured on VIS ellipsometry. The only fitting parameters during the normal fit were n and k of the dielectric layer. Fit was set in range of 2.5 to 20 μm.

In conclusion, selected characterization methods provide sufficient optical information about measured sample. The accuracy of the results mostly depend on carefulness of analytical work with data. These outcomes are presented in upcoming chapter.

3. Waveguide optimization

The main task of this chapter is to present and evaluate most of the results achieved during the research. While previous chapters have paved the way for better theoretical and technical understanding of the outlined topic and showed direct results of used fabrication and characterization methods, this chapter deals with main tasks of the thesis, which is to evaluate focused dielectrics for mid-infrared waveguides, using fabrication processes available at CEITEC infrastructure. Since most of the work is based on materials and final waveguide product is achieved without laser and detector implementation, functional demonstration will be presented through simulations.

3.1 Refractive index and Losses of different dielectrics

In chapter MIR-Waveguides optical properties of SiO_2 and Si_3N_4 are discussed. Some of these measurements investigated samples that were fabricated at TU Wien, achieved transparency for SiO_2 up to 6 μm and for Si_3N_4 up to 7.3 μm, Figure 3.1 and 3.2 show data measured on samples produced at CEITEC facility.

Figure 3.1 compares values of deposited layers from magnetron sputtering, PECVD and ALD with database values [11]. All three samples were deposited onto the Si wafer mentioned in a substrate section. The temperature for magnetron sputtering and PECVD was 100 °C, while ALD worked at 200 °C. The choice of temperature was determined by PECVD instrument, since it is calibrated for 100 °C. VIS and MIR ellipsometers were utilized to measure these samples. The experimental data were fitted into the model, consisting of two layers. Silicon substrate and deposited dielectric layer. During the normal fit, the only fitted parameter was refractive index and extinction coefficient for given dielectric. The further information can be found in VIS and MIR ellipsometry section. For experimental data with high noise, generic oscillator layer fitting was utilized instead of n & k. This method uses previously executed point-by-point fit as a reference material. Oscillators of specified energy, width and amplitude are added to the layer. In order to achieve the lowest possible MSE, fit to the reference is performed. It is further improved by other parameters adjustment. At the end normal fit is executed. Such a method has several advantages. Since the solution is in a form of continuous function. Unlike previous method, n and k can be calculated for every choice of λ without need of interpolation.

The results of refractive index n correspond well to the database, just as extinction coefficient k on the large scale. However, the detailed view at desired location, showed in inset placed in the top left corner of k on λ dependence, reveal significantly higher values, that would have unpleasantly affected the propagation length through

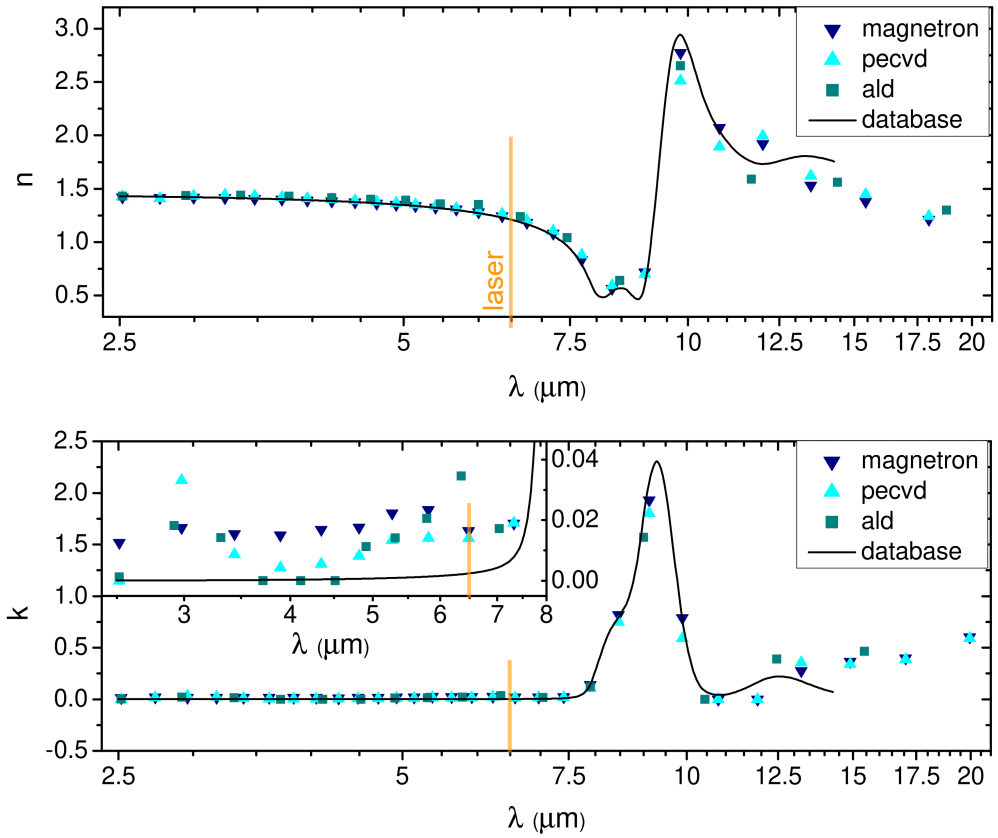

Figure 3.1: Thin layer measurement of deposited SiO_2 at 100 °C for magnetron sputtering, 100 °C for PECVD and 200 °C for ALD. All samples made at CEITEC. This figure shows refractive index n and extinction coefficient k dependence on wavelength λ.

the waveguide. In case of magnetron sputtering and PECVD, this can be resulted by high porosity coming from relatively low deposition temperature, since deposited atoms do not have enough energy to move around the surface to fill the holes created during the deposition. In addition, sample from magnetron sputtering is slightly contaminated by working gas and PECVD by gasses involved in chemical reactions. Phenomenon of high porosity is on the other hand very unlike for ALD, as this method utilizes atomistic deposition with given crystallographic structure. In this case increase has to be mainly caused by contamination, likely in the form of H2O.

Figure 3.2 compares values of deposited layers using PECVD with database values [11]. Si_3N_4 deposition could not be performed at magnetron, since Si_3N_4 target was not available. Regards to the PECVD, the main limitation of Si_3N_4 is imprecise nitrogen to silicon ration, hence compound is rather labeled SiNx. This may radically affect n and k dependence.

The results confirm prior predictions. The n to λ dependence is significantly moved to lower values and follows very roughly the database curve. Extinction coefficient k on large scale approximately meets expected values. The detailed view in the area of interest, which represents the inset, unfortunately shows high values of k, contributing to the decreased propagation length. This deviation can be resulted from different silicon to nitrogen ratio, contaminants and high porosity. Based on these findings, SiO_2 layer made by PECVD is preferred technique.

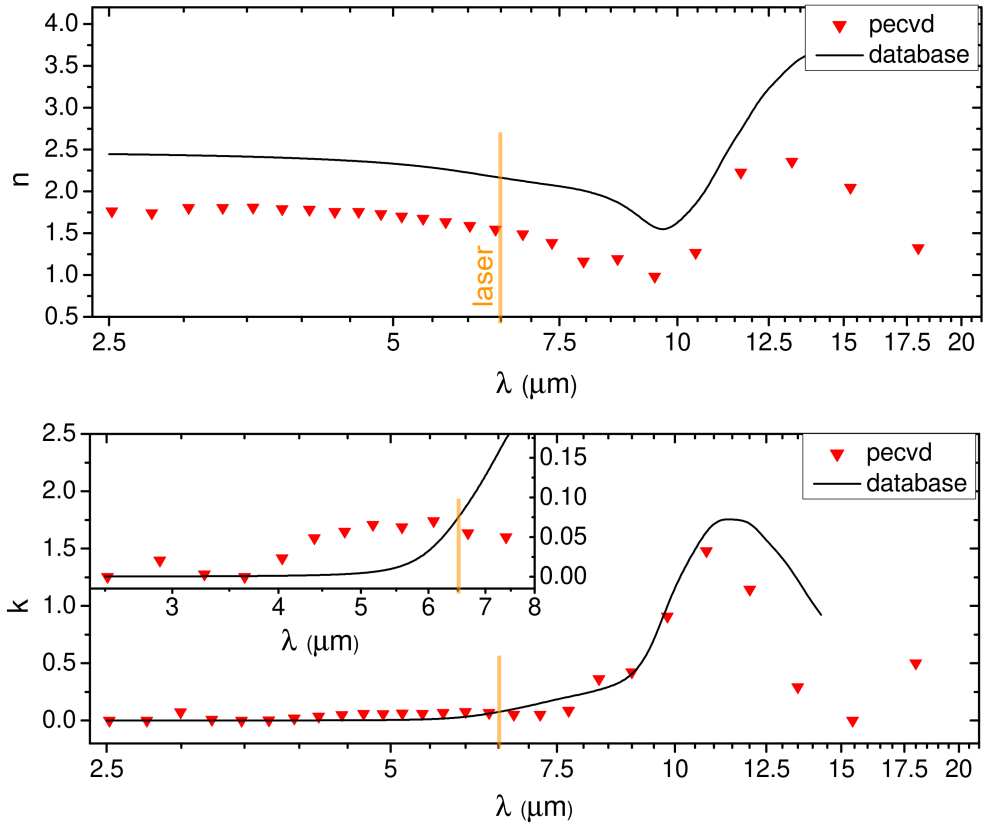

Figure 3.2: Thin layer measurement of SiNx deposited at 100 °C by PECVD technique. The sample was made at CEITEC. The figure shows refractive index n and extinction coefficient k dependence on wavelength λ.

3.1.1 Variation of deposition temperature

As discussed earlier, higher deposition temperature should decrease the extinction coefficient due to a reduction of material porosity. The main task of this section is to study extinction coefficient k of materials, that were deposited at different temperatures.

Heating at magnetron sputtering is carried out by substrate heater inside the deposition chamber. Since high temperature is only located near the substrate, due to the reduced pressure, sputtering process is not affected, enabling high temperatures. The major limitation of a heating process is the used substrate. Since substrate holder can carry only 4 inch wafers and used substrate diameter has 2 inches, attachment to the standard 4 inch wafer has to be performed. The attachment was done by Kapton tape, which is recommended to be used up to 300 °C. Due to the troubles with substrate heater, deposition only took place at 20, 50 and 100 °C. The data for $\lambda = 6.5\,\mu$m at 20 and 100 °C are shown in Table 3.1. 100°C temperature caused 2 times lower extinction coefficient k compared to the the room temperature.

The PECVD instrument is calibrated for 100 °C. Increased/decreased temperature changes the kinetics of individual chemical reactions, resulting unpredictable deposition rates and layer quality. Since no prior experimental work on parameters calibration have been recorded at higher temperatures, deposition at 200 °C was executed with retained generators and flow of the gas parameters. The data for $\lambda = 6.5\,\mu$m at 100 and 200 °C are shown in Table 3.1. The extinction coefficient for 200 °C is a little higher than for 100 °C, therefore SiO_2 at 100 °C have been used for the waveguide fabrication.

Table 3.1: Measured values of extinction coefficient k for different temperatures at $\lambda = 6.5\,\mu$m

material	method	lab	T [°C]	k
SiO_2	pecvd	TU Wien	300	0.006
Si_3N_4	pecvd	TU Wien	300	0.001
SiO_2	magnetron	CEITEC	20	0.037
SiO_2	magnetron	CEITEC	100	0.019
SiO_2	pecvd	CEITEC	100	0.015
SiO_2	pecvd	CEITEC	200	0.017
Si_3N_4	pecvd	CEITEC	100	0.081
SiO_2	ald	CEITEC	200	0.022

3.1.2 TiO2 - Emerging concept

In the past weeks, TiO_2 target was placed into the magnetron chamber at CEITEC infrastructure. This material has recently become an object of investigation for many research teams. Furthermore, it seems suitable for waveguide application in mid-infrared spectrum. Hence, I decided to include TiO_2 measurement and compare it with best SiO_2 and Si_3N_4 results achieved in CEITEC laboratory. Figure 3.3 shows optical characteristic of these materials.

At the investigated wavelengths TiO_2 has almost two times higher refractive index than SiO_2, but more importantly, the same values of extinction coefficient k in an area of interest have been reached, despite the deposition temperature of TiO_2, that took place under 20 instead of 100 °C. TiO_2 could be even suitable for higher wavelengths analysis, as k does not grow so steeply. Even better results are anticipated for higher temperatures. Hence, TiO_2 is expected to be one of the most promising materials for mid-infrared waveguide application.

In regards to the substrate, InP wafers are planed to be used for waveguide fabrications, to show compatibility with established InP-based sensor chips. An ellipsometric measurement of substrate on its own was executed in order to create layer for subsequent fitting, since laboratory database did not contain such a material. Thanks to this, the process is now ready for a transfer to InP substrates.

3.2 Stripe structure waveguide

Both TIR and SPP waveguides efficiency increases with lateral confinement, resulting into the rib, ridge or stripe structure [2] [4]. The case of stripe structure SPP waveguide was already discussed in SPP waveguide chapter. Dielectric stripe was located on the surface of planar metallic layer. The fabrication of this structure was demonstrated in the lithography section utilizing photolithography technique.

In order to get an idea of propagation length on dielectric layer thickness and stripe width dependence, simulation was performed. For this purpose Lumerical software has been used, specifically Mode solutions package, that calculates waveguide eigenmodes in cross section perpendicular to the propagating direction, unlike its more popular brother FDTD (finite-difference time-domain) solutions, that monitor the propagation of electromagnetic waves through the material by numerical calculations of Maxwell

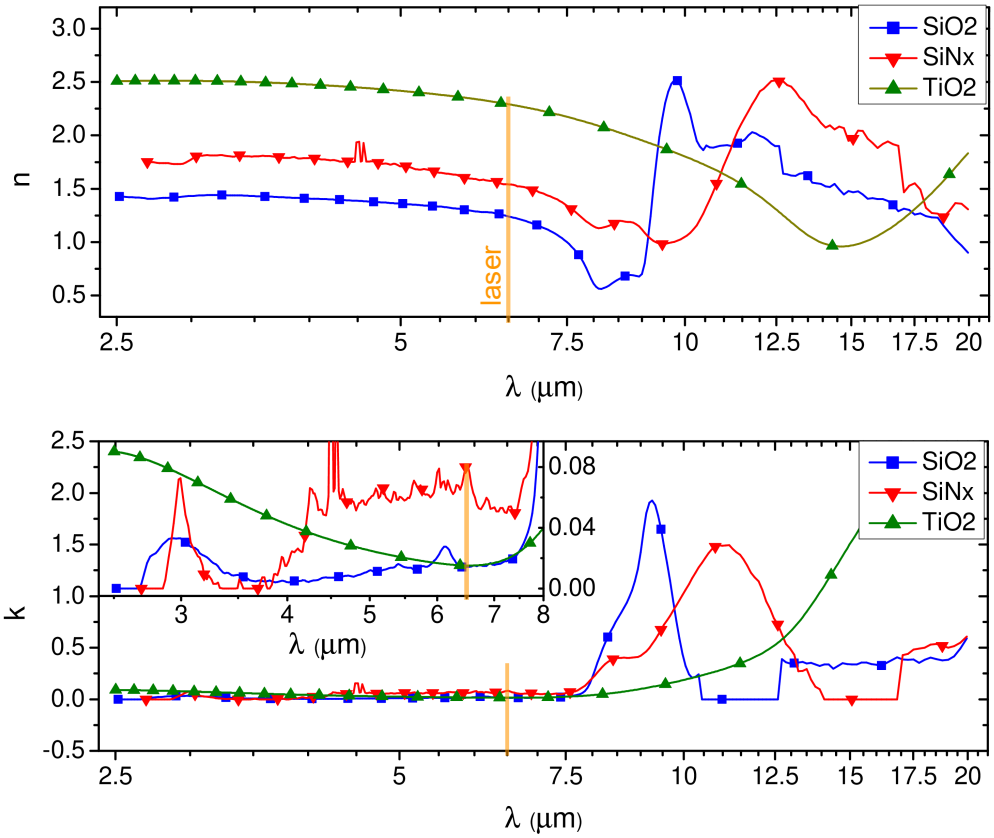

Figure 3.3: Thin layer measurement of SiO_2 deposited at 100 °C by PECVD technique, SiNx, deposited at 100 °C by PECVD technique, and TiO_2, deposited at 20,°C by magnetron sputtering. All samples were made at CEITEC. The figure shows refractive index n and extinction coefficient k dependence on wavelength λ.

equations and application of boundary conditions. In regards to the sensor efficiency, mode solution gives only approximate length estimation, since laser & detector positions and absorbances of analyzed compounds are important variables, that are not included in these calculations. The advantage of dealing with a waveguide on its own is the reduced simulation time. Where eigenmodes calculation takes only a few minutes, FDTD method can take a few days. Since the simulation has to be executed for every changed waveguide parameters, Mode solutions has been preferred over FDTD method. Optical properties of used materials were obtained from Kischkat's database [11].

Figure 3.4 shows simulated 2D mode profile for 15 μm wide and 100 nm thick dielectric stripe of SPP waveguide. The Al layer is 100 nm thick.

The propagation length reaches tens of millimeters, which is more then sufficient for on-chip implementation. Unlike SiO_2, Si_3N_4 has high refractive index n providing better confinement, on the other hand the relatively high value of extinction coefficient k at $\lambda = 6.5\,\mu$m increases wave damping. In fact, the propagation length would be significantly reduced, due to the absorption in adjacent medium, where the most part of the waveguide eigenmode is located. This reduction would have mostly affect waveguides with low confinement, reffering to the SiO_2 waveguide.

Figure 3.5 shows the penetration length dependence on dielectric stripe thickness and width. Whereas the upper line shows width dependence with constant thickness

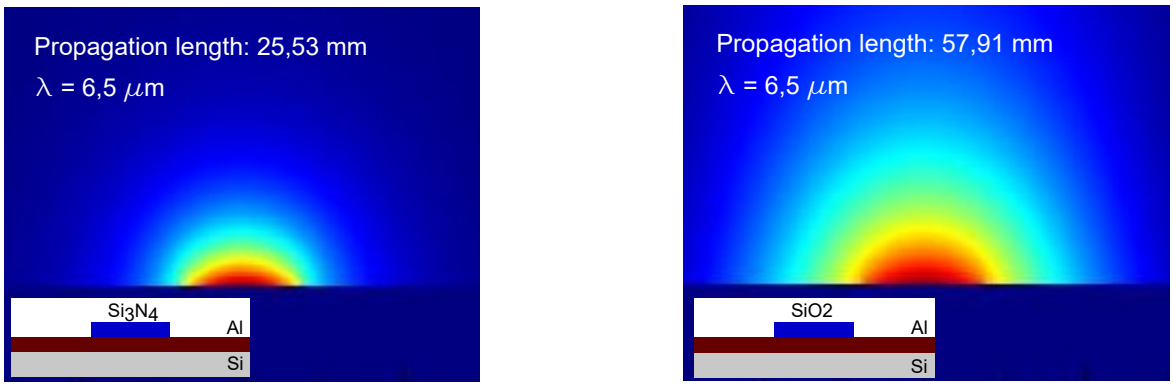

(a) Si_3N_4 (b) SiO_2

Figure 3.4: Modal field amplitude of electric intensity in waveguide cross section.

$t = 100\,\text{nm}$, the bottom line shows thickness dependence with constant width $w = 15\,\mu\text{m}$. The Al layer is 100 nm thick in all cases.

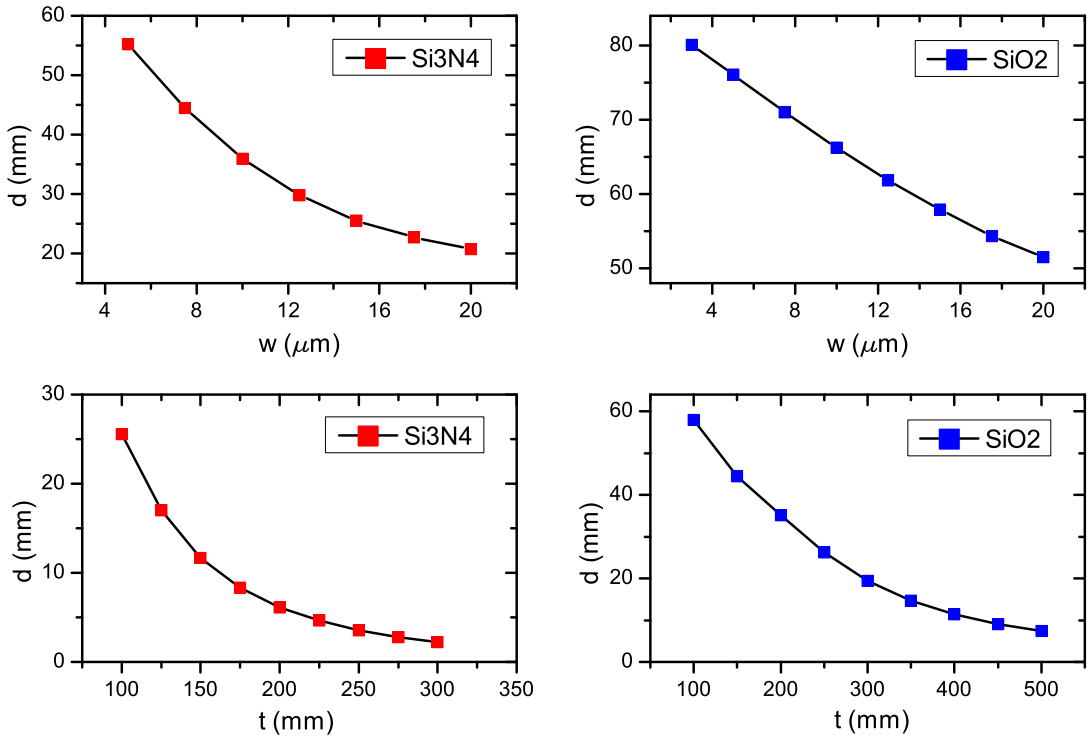

Figure 3.5: Propagation distances dependence on dielectric stripe thickness and width.

The results confirm expressed assumptions that were predicted in previous pages. Reduced stripe width, causing increased lateral confinement, lead to the longer propagation length, where reduced stripe thickness results longer propagation length, due to the damping decrease. With respect to the second statement, bear in mind, the absorption, which would have the opposite effect, have not been considered. The results also confirm, that chosen strip structure dimensions for lithography fabrication meet sufficient propagation length requirements.

Summary

This bachelor thesis considered different dielectrics for mid-infrared waveguides in regards to its sensor application. The main goal was to optimize candidates, fabricate and characterize dielectric materials. This work was mainly concerned with silicon-based compounds, as they are commonly used in research and industry.

The first chapter described two independent wave-guiding concepts, serving as a region of interaction with analyzed substances. TIR waveguides have been compared to SPP waveguides and reviewed as insufficient for device miniaturization and detection of substances with low absorption or low concentration. In this chapter there are also defined desired optical characteristics of dielectrics and presented few possible materials.

The second chapter dealt with fabrication techniques of thin layer deposition, magnetron sputtering and PECVD. There were described ellipsometry for optical characterization, focusing on an area of interest around 6.5 μm, where lasers usually work, and photolithography, used to produce stripe structure waveguide, which was successfully demonstrated on SiO_2 stripe on Al plane structure and displayed using electron microscopy.

The third chapter evaluated properties of dielectric layers in regards to a deposition technique and temperature. In particular, the low loss characteristics of observed material were emphasized. Considering SiO_2, PECVD showed slightly lower extinction coefficient values in a region of interest than magnetron sputtering. In relation to the temperature, only few measurements were made owing to the wafer and PECVD temperature limitations. While extinction coefficient of magnetron sputtering samples was improved for higher temperatures, PECVD showed best results for 100 °C. In regards to the Si_3N_4, it suffered from high extinction coefficient in observed wavelength range, on the other hand SiO_2 waveguide met the requirements. The simulation showed propagation length reaching tens of millimeters. In the end, emerging alternative in form of TiO_2 was introduced and compared to the Si-based dielectrics, showing promising results.

List of Abbreviations

AC ..... Alternating current

ALD ..... Atomic layer deposition

CVD ..... Chemical vapor deposition

DC ..... Direct current

FDTD ..... Finite-difference time-domain

MBE ..... Molecular beam epitaxy

MIR ..... Mid-Infrared

MSE ..... Mean square error

PECVD ..... Plasma-enhanced chemical vapor deposition

PVD ..... Physical vapor deposition

RF ..... Radio frequency

SPP ..... Surface plasmon polariton

TIR ..... Total internal reflection

Bibliography

[1] Mizaikoff, B. Waveguide-enhanced mid-infrared chem/bio sensors. *Chemical Society Reviews*, 42 (22), **2013**, pp. 8683–8699.

[2] Sieger, M. and Mizaikoff, B. Toward On-Chip Mid-Infrared Sensors. *Analytical Chemistry*, 88 (11), **2016**, pp. 5562–5573.

[3] Schwarz, B., Reininger, P., Detz, H., *et al.* Monolithically integrated mid-infrared quantum cascade laser and detector. *Sensors (Switzerland)*, 13 (2), **2013**, pp. 2196–2205.

[4] Schwarz, B., Reininger, P., Detz, H., *et al.* Monolithically integrated mid-infrared lab-on-a-chip using plasmonics and quantum cascade structures. *Nature Communications*, 5 (1), **2014**, pp. 1–7.

[5] Maier, S. A. *Plasmonics: Fundamentals and applications.* Springer, 2007, pp. 3–220.

[6] Kittel, C. *Introduction to solid state physics*, vol. 2. J. Wiley, 8th edn., 2005, p. 43.

[7] Li, F., Jackson, S., Magi, E., *et al.* Low propagation loss silicon-on-sapphire integrated waveguides for the mid-infrared. *Optics Express*, 19 (16), **2013**, pp. 15212–15220.

[8] Liang, H., Soref, R., Mu, J., *et al.* Long range mid-infrared propagation in Si and Ge hybrid plasmonic-photonic nano-ribbon waveguides. *Optics Express*, 22 (23), **2014**, p. 28489.

[9] Shao, G., Lu, Y., Hanaor, D. A., *et al.* Improved oxidation resistance of high emissivity coatings on fibrous ceramic for reusable space systems. *Corrosion Science*, 146 (November), **2019**, pp. 233–246.

[10] Dury, M. R., Theocharous, E. T., Harrison, N. J., *et al.* The NPL wide-area MIR calibration source. *Thermosense XXVI*, 5405 (June), **2004**, p. 532.

[11] Kischkat, J., Peters, S., Gruska, B., *et al.* Mid-infrared optical properties of thin films of aluminum oxide, titanium dioxide, silicon dioxide, aluminum nitride, and silicon nitride. *Applied optics*, 51 (28), **2012**, pp. 6789–98.

[12] Blažková, N. *Fakulta chemická.* diplomová práce, VUT, 2018.

[13] Metzler, M. and Patel, R. *Plasma Enhanced Chemical Vapor Deposition (PECVD) of Silicon Dioxide (SiO2) Using Oxford Instruments System 100 PECVD Plasma Enhanced Chemical Vapor Deposition (PECVD) of Silicon.* Tech. rep., Singh Center for Nanotechnology, Penn, 2017.

[14] Metzler, M. and Patel, R. *Plasma Enhanced Chemical Vapor Deposition (PECVD) of Silicon Nitride (SiNx) Using Oxford Instruments System 100 PECVD Plasma Enhanced Chemical Vapor Deposition (PECVD) of Silicon.* Tech. rep., Singh Center for Nanotechnology, Penn, 2017.

[15] Ohring, M. *The Materials Science of Thin Films.* Academic Press, 1992, p. 703.

[16] Levinson, H. J. and Arnold, W. H. *Optical Lithography.* 1997, p. 11.

[17] Reininger, P., Andrews, A. M., Schuler, S., *et al.* Origin of secondary-electron-emission yield-curve parameters. *Journal of Applied Physics*, 46, **1975**, p. 3347.

[18] Hilfiker, J. N. and Linford, M. R. A Review of Tompkins' and Hilfiker's Book Entitled: 'Spectroscopic Ellipsometry: Practical Application to Thin Film Characterization'. (July), **2018**, pp. 2–7.

[19] Hilfiker, J. N., Pribil, G. K., Synowicki, R., *et al.* Spectroscopic ellipsometry characterization of multilayer optical coatings. *Surface and Coatings Technology*, 357 (June 2018), **2019**, pp. 114–121.

[20] Woollam, J.A., C. *Guide to Using WVASE Spectroscopic Ellipsometry Data Acquisition and Analysis Software.* 1. 2012, pp. 194–195.